Food Chemistry: X 24 (2024) 101797

Contents lists available at ScienceDirect

Food Chemistry: X

journal homepage: www.sciencedirect.com/journal/food-chemistry-x

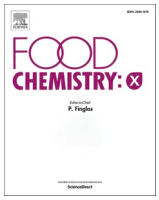

Effective extraction and detection of aflatoxins in cereals using nitrogen-rich benzodiimidazole linkage magnetic covalent organic framework based solid phase extraction and HPLC-MS/MS analysis

Dan Wei [a,b], Jianliang Li [a], Shuangshuang Zheng [a], Ming Guo [c], Jingjing Xu [a], Qiao Deng [a,*], Xu Wang [a,b,*]

[a] Hangzhou Medical College, School of Laboratory Medicine and Bioengineering, Hangzhou, 310053, China, Zhejiang 311300, China
[b] Key Laboratory of Biomarkers and In Vitro Diagnosis Translation of Zhejiang province, Hangzhou 310058, China
[c] Zhejiang Chemical Production Quality Inspection Co., Ltd, Hangzhou 310023, China

ARTICLE INFO

Keywords:
Aflatoxins
Nitrogen-rich magnetic covalent organic framework
Cereal samples

ABSTRACT

Cereals are frequently contaminated by aflatoxins (AFs). The objective of this study was to develop an efficient extraction materials for rapidly extracting and detecting AFs. A novel amino-functionalized benzodiimidazole linkage magnetic covalent organic framework (Fe_3O_4@BB-COF) was simply fabricated by one-step cyclization and aromatization. The Fe_3O_4@BB-COF, having multiple N-containing active sites, exhibited excellent extraction capability towards AFs due to synergistic interactions, including the π-π interactions, hydrogen bonding interactions, polar interactions, electrostatic interactions and Lewis acid-base interactions. The Fe_3O_4@BB-COF based MSPE method for detecting aflatoxins has advantages of simple operation, short extraction time (6 min), and low material consumption (2 mg). This method exhibited satisfactory linearity (0.05–20 μg/kg), and sensitivity (0.01–0.45 μg/L for the detection limits) and accuracy (76.8–97.1 % for recovery) and was successfully applied for extracting and detecting AFs in cereals.

1. Introduction

Aflatoxins (AFs) are a class of polar compounds with low octanol/water partition coefficient (log*P* = 0.50–1.45) (Nazhand, Durazzo, Lucarini, Souto, & Santini, 2020), having the polar moieties structures of carbonyl groups, methoxy groups and ester groups (Wang et al., 2022). These compounds, primarily produced by *Aspergillus flavus* and *Aspergillus parasiticus* (Wang et al., 2016), are carcinogenic mycotoxins posing significant hazards to human and animal health, such as the carcinogenic, teratogenic, mutagenic and atherogenic effects (Gomez, Tarazona, Mateo, Jimenez, & Mateo, 2019). The food contamination caused by AFs, especially in cereals such as corn, rice, and soybeans (Li et al., 2023), has emerged as a critical concern in the context of food safety and human health (Wang et al., 2023; Wang et al., 2023). According to the International Agency for Research on Cancer (IARC), AFs have occupied a significant position in Group A carcinogens. Aflatoxin B1 (AFB1) ranks as the first place of toxic and carcinogenic compounds and is categorized as a class I carcinogen (Martínez et al., 2023). An increase in the presence of AFs has been observed in recent years, presumably associated with the ongoing climate change, and the chronic consumption of AFs contaminated cereals, even at low concentrations, still poses a substantial threat to human health. Many countries around world have established stringent limits for the allowable residue levels of AFs. For example, the European Union set the maximum residue limits of 2.0 μg/kg, and 4.0 μg/kg for AFB1 and total AFs (Hepsag, Golge, & Kabak, 2014; Jia et al., 2023; Xu, Sun, Wang, Zhang, & Sun, 2021). Given the highly toxic nature of AFs, it is imperative to develop a simple, sensitive and efficient method to monitor AFs levels in cereals, thereby safeguarding human health and food security.

Because of the cereal matrix interferences and trace levels of AFs, an efficient sample pretreatment prior to instrumental analysis is an indispensable step to achieve the accuracy and sensitivity of AFs detection (Kuang et al., 2023; Ni et al., 2022; Zhao et al., 2023). More recently, various sample pretreatment approaches used for extracting food contaminants, involving solid phase extraction (SPE) (Wang, Li, Wang, Wu, & Shi, 2023; Yu et al., 2013), magnetic solid phase extraction (MSPE) (Li et al., 2019; Zhao et al., 2020; Zhou et al., 2023), immunoaffinity column (IAC) (Maggira, Ioannidou, Sakaridis, & Samouris,

* Corresponding authors at: Hangzhou Medical College, School of Laboratory Medicine and Bioengineering, Hangzhou, 310053, China, Zhejiang 311300, China.
E-mail addresses: dengqiao@hmc.edu.cn (Q. Deng), wangxu@hmc.edu.cn (X. Wang).

https://doi.org/10.1016/j.fochx.2024.101797
Received 26 April 2024; Received in revised form 18 August 2024; Accepted 28 August 2024
Available online 31 August 2024

2021) and QuEChERS (Annunziata et al., 2017), rely on the efficient extraction adsorbents materials. As a result of their excellent properties, such as plentiful active sites, adjustable pore structures, highly chemical stability and adsorption properties, covalent organic frameworks (COFs) have emerged as excellent sorbents for the preconcentration of target molecules from various samples (Bagheri et al., 2022). As to effectively extracting these polar AFs, it is reasonable to infer that the adsorbents should have appropriate polarity (Peng et al., 2024). An effective approach to achieve suitable polarity and sufficient binding sites is through surface modification of COFs. Specifically, the introduction of polar groups or atoms, such as nitrogen containing atoms or groups, can strengthen the affinity of COFs towards AFs through the hydrogen bonds, electrostatic interactions, Lewis acid-base interaction, and hydrophilic interactions (Rezaeefar et al., 2022). Furthermore, the integration of COFs with Fe_3O_4 magnetic nanoparticles facilitates efficient and rapid isolation (Yang et al., 2023; Yang, Huang, You, & Yamauchi, 2023). Consequently, the design and synthesis of stable, nitrogen-riched magnetic COFs are highly desirable for the effective extraction of AFs from cereals. While numerous studies have been recently conducted on the synthesis of single amino-functionalized or other nitrogen-rich COFs using the postmodification strategy (Nguyen et al., 2022), there is still a relative few researches on the facile synthesis and application of magnetic COFs functionalized with multiple nitrogen-containing groups for extracting and detecting AFs.

In this work, amino-functionalized magnetic COFs, namely Fe_3O_4@BB-COF, with stable benzodiimidazole linkage were directly fabricated through a one-step cyclization and aromatization method. The Fe_3O_4@BB-COF was subsequently utilized as the magnetic adsorbent for extracting AFs from cereal samples. Then, the structural characteristics, main extraction parameters, adsorption properties and reusability of the Fe_3O_4@BB-COF were systemically investigated. Due to the presence of multiple N-containing active sites, the Fe_3O_4@BB-COF exhibited a remarkable extraction capability towards AFs. To gain further insight into the extraction mechanism, characterization and density functional theory calculations (DFT) were employed. These results revealed that Lewis acid-base interactions, hydrophilic interactions, hydrogen bond interactions and π-π interactions played crucial roles in the interactions between Fe_3O_4@BB-COF and AFs. Finally, an efficient Fe_3O_4@BB-COF-based MSPE method was established followed by HPLC-MS/MS analysis to detect AFs in rice, corn, soybean, brown rice and buckwheat samples.

2. Materials and methods

2.1. Reagents, chemicals and samples

Acetonitrile (ACN), acetic acid and ammonium acetate, all of HPLC grade, Fe_3O_4 (purity ≥97 %), *N*,*N*-dimethylformamide (purity, 99.8 %), tetrahydrofuran (purity, 99 %), acetone (purity, 99.5 %), ammonium hydroxide (purity, 99 %), ethanol (purity, 99.5 %), 2,4,6-tris(4-formylphenyl)-1,3,5-triazine (TFPT, purity ≥95 %), 1,4-phenylenediamine (PDA, purity ≥98 %) were obtained Shanghai Macklin Biochemical Co., Ltd. (Shanghai, China). AFs standards including AFB1, AFB2, AFG1, AFG2 and AFM1 (purity ≥98 %) were purchased from Meizheng Biotechnology Co., LTD. (Beijing, China). Each of AFs standards was dissolved in 1.0 mL ACN respectively to prepare single standard solutions (1 mg/L). A mixed standard solution with different concentrations was then prepared by mixing a certain volume of each standard solution using proper solvent. All solutions were stored at 4 °C before use. Soybeans, rices and corns were purchased from supermarkets (Hangzhou, China).

2.2. Instruments

Scanning electron microscopy (SEM) analysis was performed using Sigma 300 (Zeiss, Germany). Fourier transform infrared spectroscopy (FT-IR) was obtained through a Nicolet iS20 FT-IR spectrometer (Thermo Scientific, USA). X-ray diffraction (XRD) pattern was examined using a BrukerD8 Advance diffractometer (D8 Advance, Bruker, Germany). The pore size and the Brunauer-Emmett-Teller (BET) surface were conducted on the TriStar II 3flex (Micromeritics, USA) using nitrogen adsorption-desorption methods. Vibrating sample magnetometer (VSM) was conducted to measure magnetic hysteresis loops using a Lake Shore 7404 vibrating sample magnetometer (Lake Shore, USA). X-ray photoelectron spectroscopy (XPS) investigation was conducted on Thermo escalab 250XI (Thermo Fisher Scientific, USA) to elucidate the possible adsorption mechanism. The contact angle of the materials was measured by OCA 20 instrument (Dataphysics, Germany). Thermogravimetric (TG) analysis data were obtained from TG analyzer (NETZSCH TG209F3, Germany). AFs separation and detection were conducted on a Angilent 1290 HPLC equipped with 6495 MS detector (Angilent, USA) and a Endeavorsil C_{18}UHPLC column(2.1 mm × 100 mm, 1.8 μm, Dikma, China) operated at 40 °C. The injection volume was 2 μL; The mobile phase A: 5 mmol/L ammonium acetate aqueous solution, and the mobile phase B: 100 % ACN. The flow rate of mobile phase was set at 0.4 mL/min. The gradient conditions were as follows: 80 % A at 0 min, to 5 % A at 5 min, to 80 % A at 6 min. Before the next chromatographic run, the column was re-equilibrated for 4 min using the initial composition of the mobile phase.

The optimal MS parameters were as follows: mode, multiple reaction monitoring in positive (MRM^+) mode; drying gas temperature, 300 °C; sheath gas temperature, 250 °C; drying gas flow rate, 5 L/min; sheath gas flow rate, 10 L/min; nebulizer pressure, 45 psi; capillary voltage, 3500 V; and nozzle voltage, 0 V. High-purity nitrogen was used as the drying gas, sheath gas, and nebulizer gas. The MS parameters for AFs were shown in Table S1.

2.3. Preparation of Fe_3O_4@BB-COF

The Bandrowski's base (BB) monomer was successfully synthesized from 1,4-phenylenediamine (PDA) according to the previous reported method (Li et al., 2023). Briefly, 10 g of PDA was introduced into a mixed solution containing 3 mL ammonium hydroxide and 300 mL deionized water under stirring. Subsequently, 3 % H_2O_2 (120 mL) was added and the solution was stirred for 24 h under room temperature. The obtained monomer was filtered, dried at 50 °C under vacuum overnight. This pure BB was collected for the fabrication of Fe_3O_4@BB-COF.

Afterward, Fe_3O_4@BB-COF was synthesized as the following the procedures. Specifically, Fe_3O_4 (300 mg), BB (239 mg) and 2,4,6-tris(4-formylphenyl)-1,3,5-triazine (TFPT) (197 mg) were dispersed in a mixture of mesitylene (10 mL) and 1,4-dioxane (10 mL) by sonication for 20 min. Afterwards, 2 mL of acetic acid/mesitylene/1,4-dioxane solution (*v*/v/v, 30/85/85) was slowly added, and the mixture was sonicated for 10 min. The mixture was maintained at 80 °C for 3 d. The resulting dark powder was isolated through filtration, and subsequently rinsed using dimethylformamide, tetrahydrofuran, acetone and ethanol until the supernatant was colorless, and then dried under vacuum at 60 °C overnight.

2.4. Fe_3O_4@BB-COF-based MSPE procedure

Each soybean, rice, corn, brown rice and buckwheat sample was thoroughly ground and mixed using a grinder or mincing machine, then 5 g of each sample was placed in centrifugal tubes, and 10 mL of an aqueous solution containing 80 % ACN by volume was added, vortexed and sonicated to completely dissolve and extract the target AFs. After 10 min of centrifugation at 10, 000 rpm/min, the supernatant was collected for the subsequent MSPE procedures.

2 mg Fe_3O_4@BB-COF was dispersed into a 2 mL centrifuge tube containing 1 mL of the mixed standard solution or the spiked sample solution. The mixture was vortexed for 1 min to achieve complete adsorption of the AFs from the solution onto the Fe_3O_4@BB-COF. Then

the Fe_3O_4@BB-COF was isolated using an external magnet. Subsequently, 1 mL ACN was added as eluent and vortexed for 5 min. Finally, the eluate was filtered through a 0.22 μm membrane filter before HPLC-MS/MS analysis.

2.5. Statistical analysis and DFT calculations

Statistical analysis was conducted using Origin 2021 software (OriginLab Software, Northampton, MA, USA). DFT calculations were performed on the latest version of ORCA quantum chemistry software (Version 5.0.4). The structures of the molecules including five AFs, BB-COF and the representative periodic fragment of BB-COF were fully optimized at the BLYP functional and the def2-SVP basis. The singlet point energy calculations were performed with B3LYP functional and a larger basis set namely def2-SVP basis set. The color-filled isosurface graphs were used to visualize themolecular electrostatic potential (MESP) and molecular sizes for all the molecules.

3. Results and discussions

3.1. Characterization of Fe_3O_4@BB-COF

The morphology of Fe_3O_4@BB-COF were investigated by SEM (Fig. 2a). As shown in Fig. 2a, Fe_3O_4@BB-COF exhibited a spherical shape with slight degree of aggregation, measuring approximately 200 nm in diameter. The presence of rougher surface of Fe_3O_4@BB-COF nanosphere indicated the successful coating of BB-COF layers onto the surface of Fe_3O_4 nanoparticles. (See Fig. 1.)

The FT-IR spectra of PDA, BB, TFPT and Fe_3O_4@BB-COF were illustrated in Fig. 2b. The newly emerged peak at 1614 cm^{-1} in the FTIR spectrum of BB, when compared to the FTIR spectrum of PDA, was attributed to the presence of –C=N– bonds. This observation provided evidence for the successful synthesis of the BB monomer. In the FTIR spectrum of Fe_3O_4@BB-COF, the –CHO peak (1700 cm^{-1}) of TFPT disappeared, and the newly appeared vibration peak at 572 cm^{-1} and 1613 cm^{-1} were attributed to the Fe–O–Fe of Fe_3O_4 and the –C=N– bonds of the benzodiimidazole rings (Luan et al., 2022), respectively, demonstrating the successful synthesis of Fe_3O_4@BB-COF.

The crystal structure of Fe_3O_4@BB-COF was measured by XRD

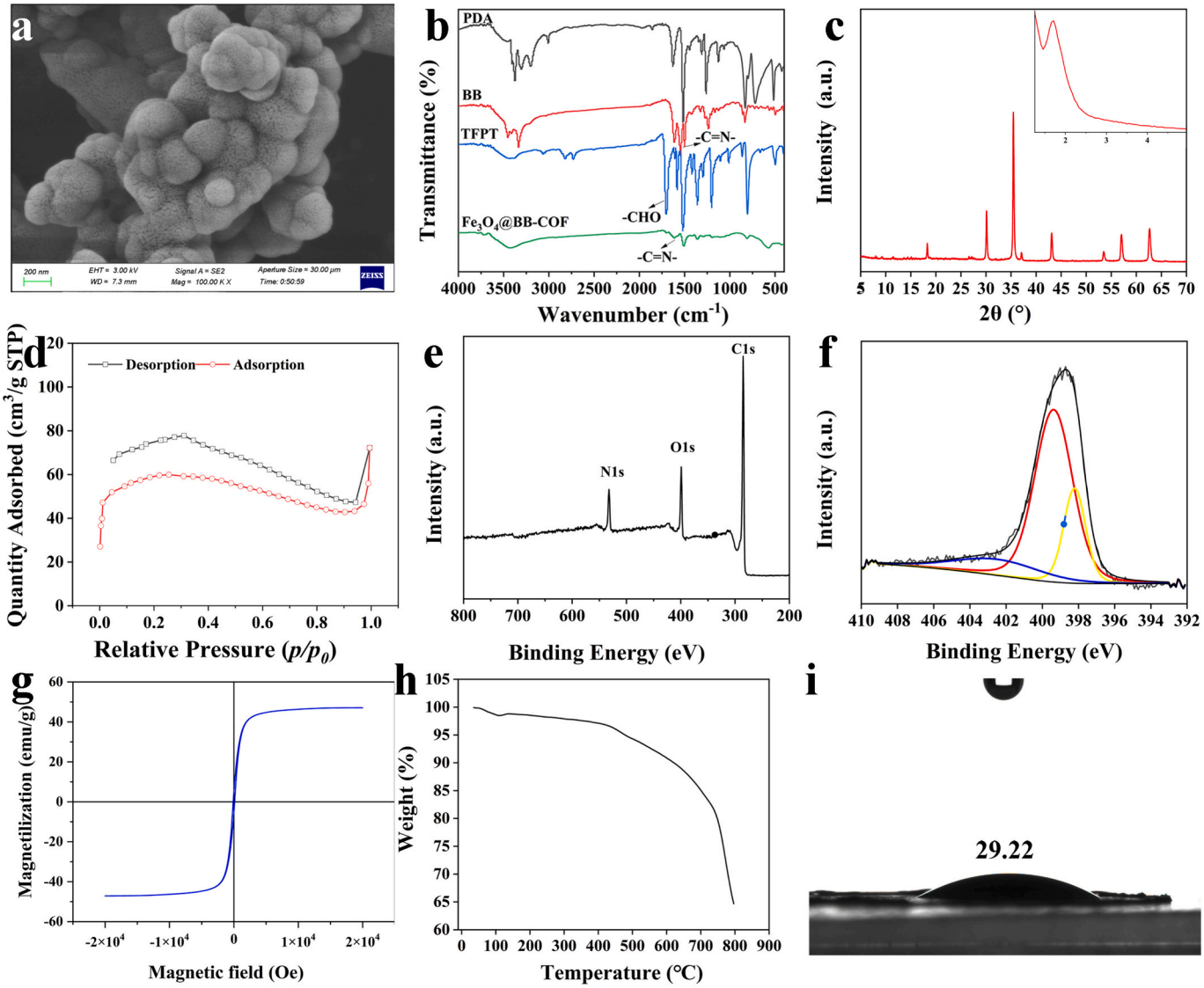

Fig. 2. (a) SEM image of Fe_3O_4@BB-COF; (b) FT-IR spectra of TFPT, BB and Fe_3O_4@BB-COF; (c) XRD spectra of Fe_3O_4 and Fe_3O_4@BB-COF; (d) the N_2 adsorption-desorption isotherms of Fe_3O_4@BB-COF; (e) XPS full scan spectra and (f) N1S spectra of Fe_3O_4@BB-COF; (g) magnetic hysteresis curves of Fe_3O_4@BB-COF; (h) TGA curves of Fe_3O_4@BB-COF; (i) the contact angle image of Fe_3O_4@BB-COF@BB-COF.

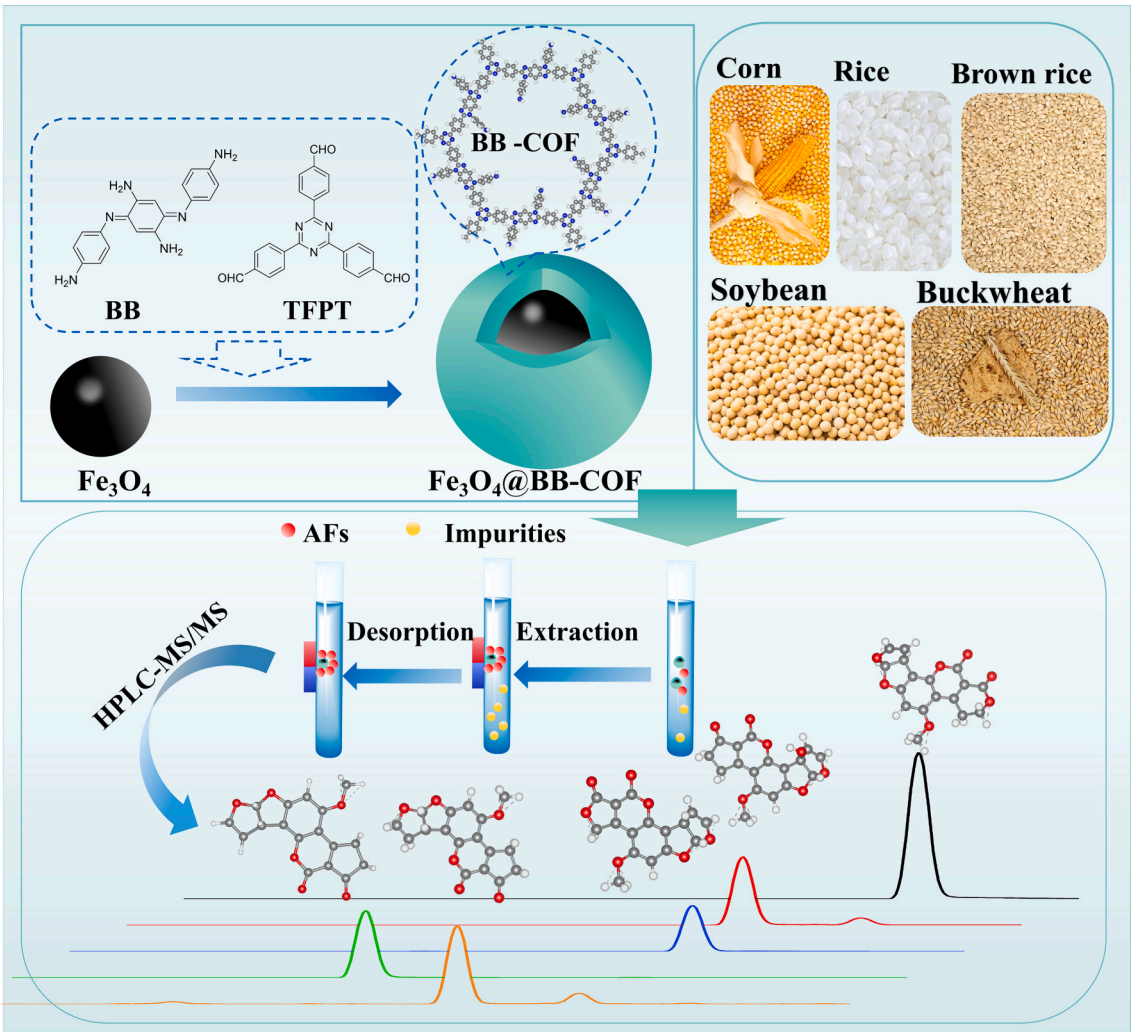

Fig. 1. Schematic diagram of the synthesis of Fe_3O_4@BB-COF and application for the MSPE and detection of AFs.

pattern in Fig. 2c, Fe_3O_4@BB-COF had a diffraction peak at 1.7°, which were ascribed to the crystallographic faces (100). Besides, the characteristic peaks at 30.3°, 35.5°, 43.0°, 53.5°, 57.0° and 62.6° were consistent with the crystallographic faces (220), (311), (400), (422), (511), and (440) of Fe_3O_4, respectively. The results indicated that Fe_3O_4@BB-COF showed the good crystallinity.

The BET analysis was carried out to evaluate the porosity characteristic of Fe_3O_4@BB-COF. The BET surface area of Fe_3O_4@BB-COF was calculated to be 66.1 $m^2 \cdot g^{-1}$ from the N^2 adsorption-desorption isotherms (Fig. 2d), and the average pore size distribution was 2.5 nm. The relatively small BET surface area of Fe_3O_4@BB-COF can be attributed to the magnetization of BB-COF. Taking into account both the adsorption and desorption efficiency, such specific surface area of Fe_3O_4@BB-COF is sufficient for effective MSPE of AFs.

In order to investigate the bonding correlation and element composition of Fe_3O_4@BB-COF, XPS spectra was employed. The XPS spectra in Fig. 2e showed the presence of C (284.57 eV), O (531.87 eV), and N (398.8 eV) elements in the Fe_3O_4@BB-COF. The N 1 s spectra can be split into three peaks of iminazole-N (398.21 eV), iminazole-N (399.37 eV) and amino-N (402.50 eV) (Fig. 2f).

To evaluate magnetic response performance, the magnetic hysteresis curve was showed in Fig. 2g. The saturated magnetization of Fe_3O_4@BB-COF was 47.06 emu/g, revealing that the magnetism of Fe_3O_4@BB-COF could favor rapid separation in MSPE procedure.

TG analysis (Fig. 2h) was used to investigate the thermal stability of Fe_3O_4@BB-COF in the range of 30–800 °C. Only a small amount (<20 %) of mass loss was observed before 741.2 °C, which can be ascribed to volatilization of the organic solvent on the surface of the material. 35.5 % weight loss of Fe_3O_4@BB-COF was observed from 797 °C, which can be ascribed to the decomposition of the BB-COF shell. The result indicated that the Fe_3O_4@BB-COF exhibited good thermal stability up to 741 °C.

The surface property of Fe_3O_4@BB-COF was measured through the contact angle experiment (Fig. 2i). The contact angle of 29.22° for Fe_3O_4@BB-COF suggested that Fe_3O_4@BB-COF is hydrophilic and favor the adsorption of polar AFs.

3.2. Optimization of MSPE procedure

3.2.1. Effect of adsorbent dosage

The dosage of the adsorbent is a crucial factor for effectively extracting target compounds from complex matrices. The dosage of Fe_3O_4@BB-COF was evaluated in a range of 0.5 to 5 mg (Fig. 3a). The results revealed that the recoveries of AFs enhanced when initially increasing the dosage of Fe_3O_4@BB-COF from 0.5 to 2 mg, but remained constant with further increasing from 2 to 5 mg, suggesting that 2 mg of Fe_3O_4@BB-COF is adequate for extracting AFs. Consequently, 2 mg of Fe_3O_4@BB-COF was chosen for the subsequent experiments.

3.2.2. Effect of sample pH

The stability of AFs is susceptible to the sample pH. Furthermore, the pH value of the sample can influence the existing forms of targets and

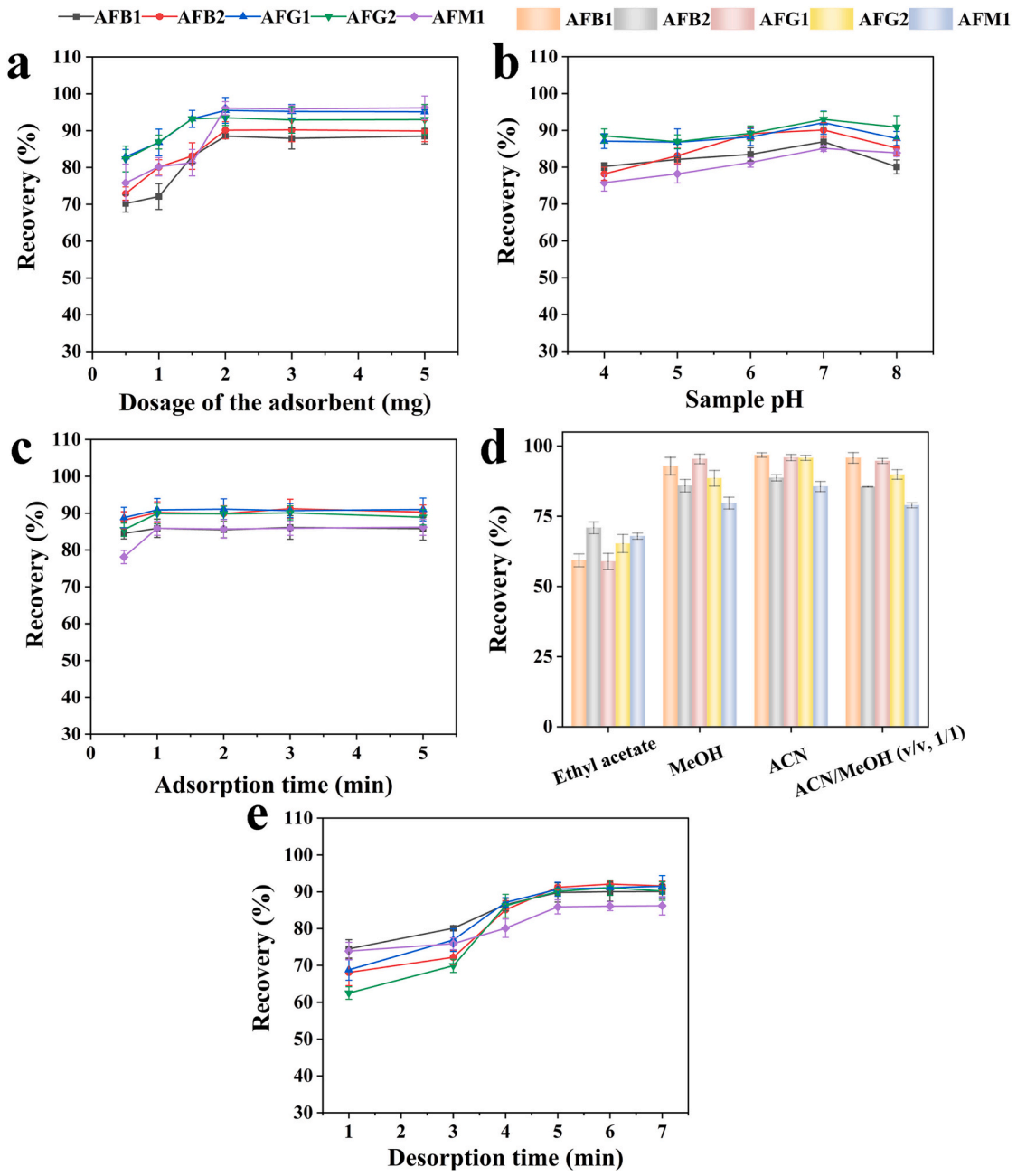

Fig. 3. Optimization of MSPE conditions: (a) dosage of adsorbent; (b) sample pH; (c) adsorption time; (d) type of eluent solvent; (e) desorption time.

interactions between the targets and adsorbents, subsequently affecting the extraction efficiency. In order to assess the optimal pH range, the sample pH was evaluated in the range of 5.0–8.0. As illustrated in Fig. 3b, the increase in recoveries of AFs was observed with the pH value of 5.0–7.0. However, a slight decrease was observed at pH 8.0, which can be ascribed to the decomposition of AFs under both acidic and alkaline conditions (Vijayalakshmi, Nadanasabhapathi, Kumar, & Kumar, 2018). Thus, sample pH was adjusted to 7 for the subsequent MSPE experiment to ensure optimal extraction efficiency.

3.2.3. *Effect of adsorption time*

Adsorption time was investigated by varying the vortex time from 0.5 to 5 min. As shown in Fig. 3c, the extraction recoveries of AFs increased from 0.5 to 1 min, subsequently maintaining a stable level when the adsorption time exceeding 1 min. The observations indicated that the extraction equilibrium can be achieved within 1 min. Thus, the optimal adsorption time for the following experiments was determined to be 1 min.

3.2.4. *Effect of the type of eluent solvent*

The impact of diverse desorption solvents, specifically ethyl acetate, MeOH, ACN, and a mixture of ACN/MeOH (*v*/v, 1/1), on the extraction efficiency was thoroughly investigated. As shown in Fig. 3d, ACN provided the best desorption efficiency. On the other hand, ethyl acetate, due to its weak polarity, demonstrated limited desorption efficiency towards AFs. Presumably, this was attributed to the hydrophilic interactions between the AFs and Fe_3O_4@BB-COF. In view of these results, ACN was selected as the desorption solvent for further experiments.

3.2.5. *Effect of desorption time*

The complete removal of analytes from the adsorbent requires adequate desorption time. The desorption time was assessed by varying

vortex time from 1 min to 7 min. As the vortex desorption time was initially prolonged from 1 min to 5 min, a distinct upward trend was observed in the recoveries of all AFs. However, further prolongation of the vortex time did not lead to any significant changes in the recoveries (Fig. 3e), indicating that vortexing for 5 min is sufficient to effectively desorb the AFs. Hence, the desorption time was set at 5 min for our experiments.

3.2.6. Reusability, stability and reproducibility of Fe_3O_4@BB-COF

The reusability of Fe_3O_4@BB-COF was evaluated in terms of MSPE recoveries under the optimal conditions. Following each MSPE circle, the Fe_3O_4@BB-COF was retrieved and sequentially washed with acetonitrile and water before reuse (Fig. S1). After 6 times uses, a reduction in recoveries by approximately 15 % was observed, which suggested that Fe_3O_4@BB-COF can be used at least 6 times. While the reusability of Fe_3O_4@BB-COF is not entirely satisfactory, the utilization of low dosages in the MSPE process can partially compensate for the limited reuse cycles in terms of cost-efficiency.

The stability and reproducibility of Fe_3O_4@BB-COF are also crucial for practical MSPE applications, and were evaluated by monitoring alterations in the the FTIR spectra and MSPE recovery after immersion in acidic (pH 3 and 5), basic (pH 8 and 10) solutions, or organic solvents (ACN). As illustrated in Fig. S2, when compared to the recoveries obtained from pristine Fe_3O_4@BB-COF (83.5–96.7 %), there is no obvious changes observed after immersion in pH 3 solution (72.8–93.6 %), pH 5 solution (76.1–96.5 %), pH 8 solution (80.6–95.1 %), pH 10 solution (77.8–95.9 %) and ACN (82.5–96.2 %). And the content of -C=N- as indicated by FTIR analysis (Fig. S3) decreased by 3.9 %, 3.4 % and 2.3 % following the immersion in solutions with pH values of 3, 5, and 8, and slightly increased by 1.2 % and 1.4 % after immersion in solutions with a pH value of 10 and in ACN. Additionally, as depicted in Fig. S4, the adsorbent after one month storage under dry conditions at room temperature exhibited comparable recovery (84.1–97.2 %) with the newly prepared adsorbent (83.5–96.7 %), further indicating its good stability and reproducibility. The aforementioned results indicated that the stability and reproducibility of the material were well maintained.

3.3. Adsorption properties

To evaluate the adsorption capabilities of Fe_3O_4@BB-COF, the adsorption isotherms and adsorption kinetics experiments were performed with AFB1 and AFM1 selected as model molecule. In the adsorption isothermal adsorption experiments, 1 mg of Fe_3O_4@BB-COF was dispersed in AFB1 and AFM1 (2 mL, pH 7.0) solutions with different initial concentrations (2–120 mg/L) and vortexed (1000 rpm) for 20 min. The adsorption capacity equation, the Langmuir model and the Freundlich model were provided in the Supplementary Material. In the adsorption kinetic adsorption experiments, 1 mg of Fe_3O_4@BB-COF was added to the mixed solution containing AFB1 and AFM1 (50 mg/L, 2 mL, pH 7.0) and vortexed (1000 rpm) for the different adsorption times (0.5–10 min), The quasi-first-order kinetic model and the quasi-second-order kinetic model were given in the Supplementary Material. All the supernatant was isolated via a magnet, followed by filtration through a 0.22 μm filter membrane before HPLC-MS/MS detection.

3.3.1. Adsorption isotherm

From the adsorption curves of AFB1 and AFM1 on Fe_3O_4@BB-COF (Fig. S5), the adsorption capacity of AFB1 and AFM1 on Fe_3O_4@BB-COF increased quickly with the enhancement of initial concentration of AFB1 and AFM1, and the maximum extraction capacity of Fe_3O_4@BB-COF was found to be 98.72 mg/g and 88.26 μg/g. The Langmuir and Freundlich models were utilized to fit the experimental adsorption data. The Langmuir model exhibited stronger correlations ($R_1^2 = 0.9743$ for AFB1 and 0.9712 for AFM1) than the Freundlich model ($R_2^2 = 0.9504$ for AFB1 and 0.9652 for AFM1) (Fig. S2 and Table S2). The results implied that the adsorption of AFB1 and AFM1 onto Fe_3O_4@BB-COF occurred primarily as a monolayer adsorption process.

3.3.2. Adsorption kinetic

The adsorption kinetics experiments were conducted to further explore the adsorption behavior of AFB1 and AFM1 on Fe_3O_4@BB-COF. As shown in Fig. S6 and Table S3, the second-order models ($R_1^2 = 0.9929$ for AFB1 and 0.9979 for AFM1) fitted the adsorption data better than the first-order models ($R_2^2 = 0.7835$ for AFB1 and 0.8072 for AFM1). The experimental maximum adsorption capacity of AFB1 and AFM1 on Fe_3O_4@BB-COF aligned more closely with the predicted results obtained from the pseudo-second-order model. The adsorption kinetic results indicated the chemical adsorption played a significant role in the adsorption process.

3.4. Extraction mechanism of Fe_3O_4@BB-COF towards AFs

As mentioned in section 3.3, the Langmuir isotherms model and the second-order kinetics model have demonstrated a good fit with the experimental results, suggesting that the adsorption AFs onto the Fe_3O_4@BB-COF surface was primarily controlled by a monolayer chemisorption process.

Further, the extraction performance of Fe_3O_4@BB-COF towards pesticides of different polarity, and nonpolar sterigmatocystin having related structure with AFB1, was evaluated to verify the polar interactions. Notably, the extraction recoveries of polar pesticides (72.3 %–93.0 %) with log *P* between −0.04 and 3.70 were much higher than that towards hydrophobic pesticide (<2.2 %) with log *P* between 4.60 and 7.40 (Fig. 4a). Additionally, even having the similar structure with AFB1, the recoveries of non-polar sterigmatocystin were lower than 60 %. The results may indicated that the polar interactions contribute a lot to the extraction mechanism of Fe_3O_4@BB-COF. The good extraction performance of Fe_3O_4@BB-COF towards such polar pesticides suggests that the selectivity of Fe_3O_4@BB-COF is not specific enough. However, the selectivity of the method can be obtained by the following approaches: selection of appropriate extraction conditions (such as material dosage, extraction time, eluent solvent), HPLC separation and tandem MS selective detection.

Furthermore, the material characterizations were conducted to investigate the extraction mechanism. Specifically, FT-IR analysis of Fe_3O_4@BB-COF before and after adsorption of five target AFs (Fig. 4b) was carried out to reveal the adsorption interactions between the Fe_3O_4@BB-COF and the five target AFs. Given that AFs contain benzene rings and O atoms while the Fe_3O_4@BB-COF is rich in benzene rings and N-containing groups, the π-π interactions could be formed between benzene rings, C=C of AFs and the benzene rings of Fe_3O_4@BB-COF (FT-IR analysis) (served as π-electron acceptor, and C=C stretch peak shifted from 1580 cm^{-1} to 1578 cm^{-1} and its content decreased from 94.1 % to 83.4 % after AFs adsorption) (Cheng et al., 2022; Li et al., 2023). In the adsorption process of AFs on Fe_3O_4@BB-COF, the hydrogen bond (N-H…O and N-H…π) interactions could be formed between O atoms and benzene rings (hydrogen acceptors) of AFs and NH_2 of the Fe_3O_4@BB-COF (hydrogen donor) (FT-IR analysis) (served as π-electron acceptor, and stretch peaks shifted from 3426 cm^{-1} to 3346 cm^{-1} and its content decreased from 87.4 % to 83.3 % after AFs adsorption). Besides, the Lewis acid-base interactions could be facilitated by –OH/C=O moieties (Lewis acid) on AFs and the presence of nitrogen atoms in the iminazole-N, pyridine-N or amino-N (Lewis base) of the Fe_3O_4@BB-COF (confirmed by FT-IR analysis, C=N, C—N stretch peaks shifted from 1615 cm^{-1}, 1292 cm^{-1} to 1612 cm^{-1}, 1297 cm^{-1} and the content of C=N, C—N decreased from 93.9 %, 94.6 % to 83.0 %, 83.6 % after AFs adsorption). Additionally, these interactions were also verified by XPS spectra of Fe_3O_4@BB-COF before and after adsorption of five target AFs. Obviously, the contents of N1s in Fe_3O_4@BB-COF decreased from 15.5 % to 12.6 % in Fe_3O_4@BB-COF after AFs adsorption (Fig. 4c), and the binding energies of N1s of pyridine-N, iminazole-N, amino-N for Fe_3O_4@BB-COF after AFs adsorption were lower than that

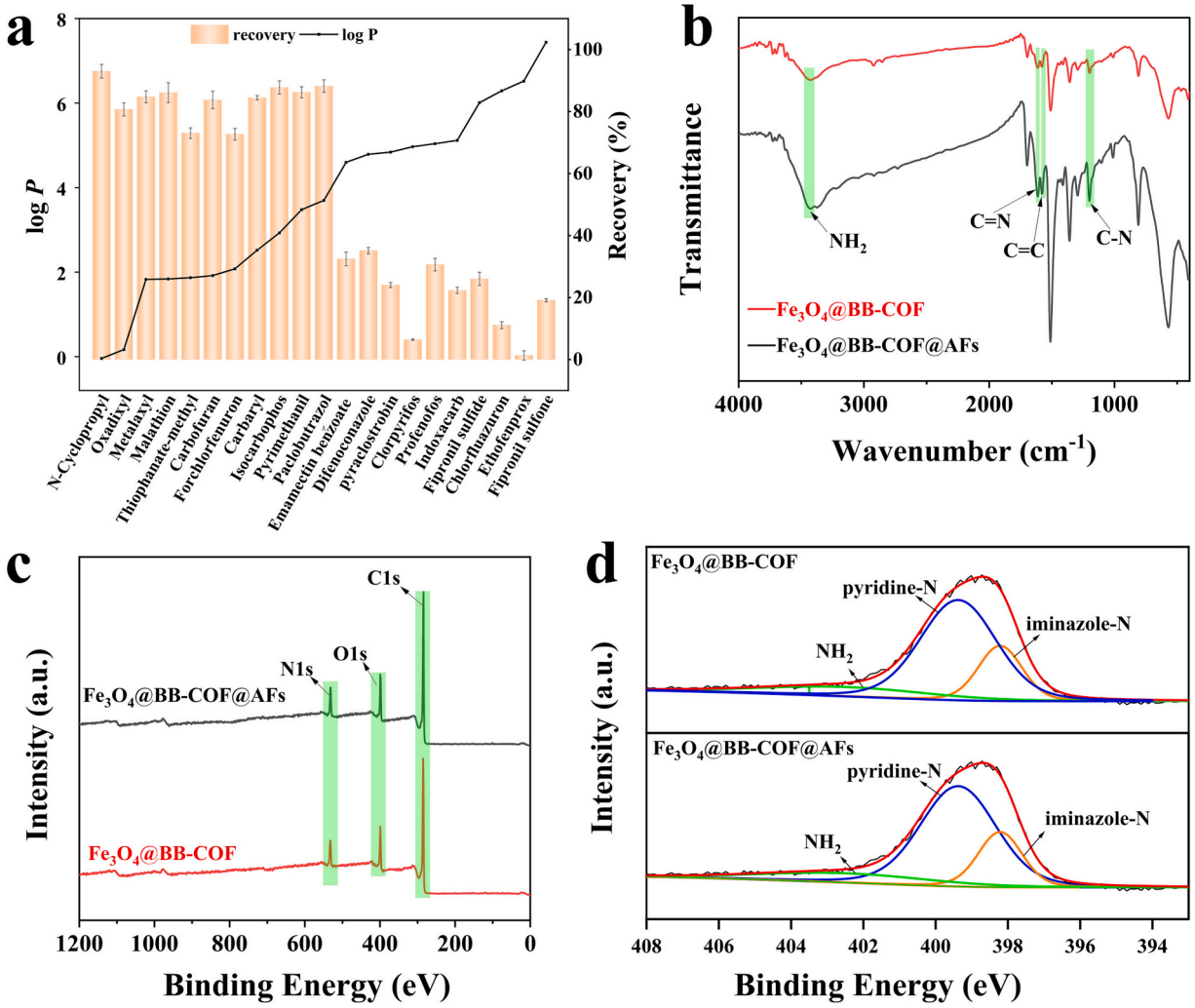

Fig. 4. (a) Recoveries of pesticides with different polarity; (b) FT-IR spectra of Fe_3O_4@BB-COF before and after the adsorption of AFs; (c) XPS full-scan spectra of Fe_3O_4@BB-COF before and after adsorption of five target AFs; (d) NS1 spectra of Fe_3O_4@BB-COF before and after adsorption of AFs.

for Fe_3O_4@BB-COF. The binding energies of pyridine-N, iminazole-N, and amino-N were changed from 399.1 eV, 398.1 eV, 402.6 eV in Fe_3O_4@BB-COF to 398.9 eV, 398.0, and 400.5 eV in Fe_3O_4@BB-COF@AFs (Ma et al., 2024) (Fig. 4d).

Finally, DFT calculations were performed to reveal the adsorption mechanism. The detailed DFT calculations were described in Supplementary Material. Firstly, the optimal configurations of five AFs and the BB-COF were utilized to calculate the molecular sizes of BB-COF and five AFs. The pore sizes for the BB-COF (24.2 Å, consistent with the BET results indicating the pore diameter of 2.5 nm) were larger than each molecular size of five AFs (8.1–11.3 Å), indicating that the synthesized BB-COF could provide a channel for AFs (Fig. 5) (Wang, Li, Wang, et al., 2023; Ma et al., 2024). Secondly, the molecules electrostatic potential (MESP) of five AFs, BB-COF and periodic BB-COF fragment were visualized (Fig. 6). AFs exhibited significant electropositivity within the potential region and their negative charge distribution were mainly localized around O atoms. In contrast, BB-COF demonstrated significant electronegativity where facilitate electrostatic interactions (negative charge region, especially the iminazole-N groups, acted as electron donor), hydrogen bonding interactions (the NH_2 groups were H donors), and the Lewis acid-base interactions (the pyridine-N, the iminazole-N and the NH_2 groups served as Lewis base) (Yang et al., 2023) with AFs (positive charge region played as electron acceptor, C=O/C-H/-OH acted as Lewis acid, O atoms were H acceptors). Finally, AFB1 was selected as model molecules and the fragment of BB-COF (Fig. 6) was employed to simulate the periodic structure of BB-COF to calculate the adsorption energy between AFB1 and BB-COF. The optimal molecular structures of AFB1 adsorbed on its periodic fragment part of BB-COF through different sites including iminazole-N, pyridine-N, and NH_2 was shown in Fig. 6. The adsorption energies (E_{ads}) (Fig. S7) of AFB1@BB-COF complexes were all negative with orders as below: $E_{(pyridine\text{-}N)} = -0.920$ eV< $E_{(iminazole\text{-}N)} = -0.793$ eV < $E_{(NH2)} = -0.178$ eV, indicating that the adsorption process is an stable and exothermic process (Yang, Ma, et al., 2023), and adsorption of AFs may preferentially occur in pyrrolic-N and iminazole-N sites of BB-COF. The results demonstrated that the abundant nitrogen-containing functional groups, pyrrolic-N and iminazole-N or NH_2 could facilitate the extraction performance of BB-COF towards AFs.

Based on the aforementioned results, it is evident that the structure characteristics of both AFs and Fe_3O_4@BB-COF determine the extraction efficiency and the extraction process of AFs by Fe_3O_4@BB-COF is associated with multiple interactions, involving pore-size matching effects, π-π interactions, hydrogen bonding interactions, polar interactions and the Lewis acid-base interactions. These multiple physicochemical forces collectively guaranteed its extraction efficiency and selectivity.

3.5. Method validation

The analytical performance of the developed Fe_3O_4@BB-COF based MSPE-HPLC-MS/MS method was evaluated by testing the spiked blank

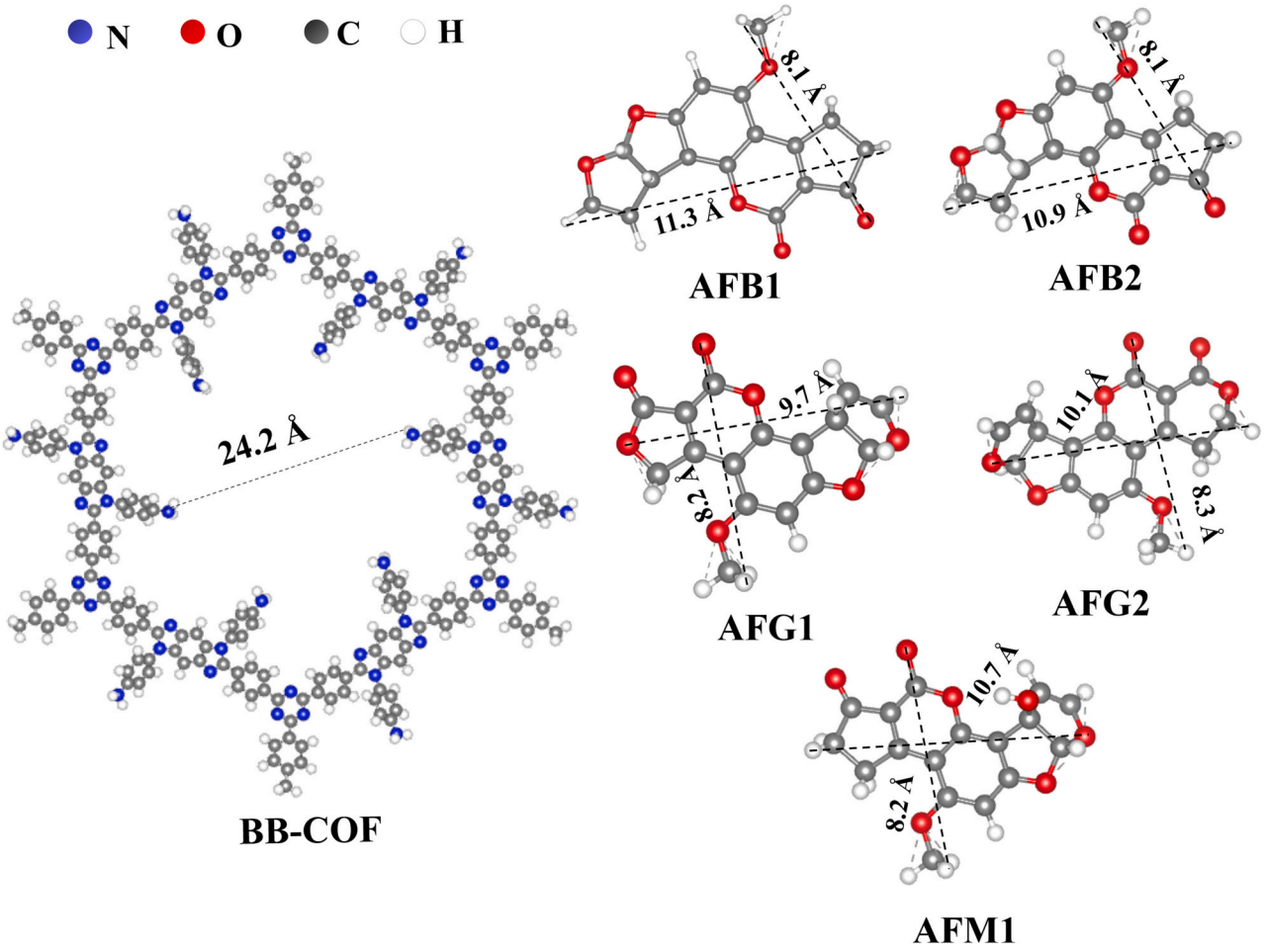

Fig. 5. The optimal molecular structures of BB-COF and five AFs.

soybean, rice and corn samples in terms of linearity, limit of quantification (LOQs, S/N = 10), limit of detection (LODs, *S/N* = 3), and intraday and interday relative standard deviation (RSD) (Table 1). The method had a good linear range between 0.05 and 0.90 (AFB1) or 0.20–0.50 (AFB2) or 0.05–1.00 (AFG1) or 0.10–1.50 (AFG2) or 0.05–1.00 (AFM1) to 20 μg/kg with determination coefficient R^2 values exceeding 0.9955. The LODs and LOQs were 0.01 μg/L-0.45 μg/L and 0.05 μg/L-1.50 μg/L, respectively. The intraday and interday RSDs (n = 5) for determining the spiked (10 μg/L) blank samples were 1.6–6.1 % and 2.0–10.2 %, respectively.

3.6. Cereal samples analysis

In order to evaluate the practical applicability of this method, a variety of cereal samples (soybean, rice, corn, brown rice and buckwheat) were determined under optimal conditions. Matrix effects (MEs) were determined by the slopes of calibration curves of each molecule in blank matrix with that in standard solutions. ME values in the range of 0.80–1.20 were generally considered to be negligible (Liu, Ling, Zhang, Feng, & Zhang, 2023). In this study, the ME values were in the range of 0.80–1.13, except for AFG1 (0.73) in soybean, AFG2 (0.65) in rice, AFB1 (0.62), AFB2 (0.68), AFG1 (0.70) and AFG2 (0.79) in corn, AFB2 (0.66) in buckwheat. The results indicated a minor matrix suppression interference existed in this method. Then, the matrix-matched calibration curves were established (Table 1) and applied for the detection of AFs residues in the actual sample detection and no target AFs was detected in real cereal samples. Furthermore, three level spiked blank samples (2, 5, 20 μg/kg) were used to assess the precision of the proposed method. The results in Table 2 showed that the recovery ranged from 76.8 % to 97.1 %. Therefore, the proposed method exhibits good linearity, precision, and accuracy.

3.7. Method comparison

The Fe_3O_4@BB-COF-based MSPE-HPLC-MS/MS method for the extraction and detection of AFs were compared with previous reports (Table S4) (Li et al., 2019; Maggira et al., 2021; Wang et al., 2023; Wang, Li, Wang, et al., 2023; Yu et al., 2013; Zhao et al., 2020; Zhou et al., 2023) in terms of analytical method, adsorbent dosage, extraction time, LOQs, recoveries and applicability (sample matrix). When comparing the Graphene oxide and F-COF based SPE or AflaM1 affinity column based IAC method, Fe_3O_4@BB-COF-based MSPE has advantages of simple operation, easy isolation (avoiding procedures of column packing or centrifugation) and low consumption of sample volume, adsorbent and solvent, and less extraction time. Compared with the Fe_3O_4@UiO-66-NH_2@MON, Fe_3O_4@MWCNTs-NH_2, PEGylated multi-walled carbon nanotubes, Fe_3O_4@COF(TAPT–DHTA) based MSPE methods, the current method requires a smaller amount of adsorbent. In terms of extraction time, the MSPE procedure employed in this method reduces the overall extraction and desorption time, less than or comparable to that of the Fe_3O_4@UiO-66-NH_2@MON, Fe_3O_4@MWCNTs-NH_2, PEGylated multi-walled carbon nanotubes, Fe_3O_4@COF(TAPT–DHTA) based MSPE methods. Moreover, the recoveries achieved by this method are comparable or even better than that of other method. Although LOQs were higher than that of AflaM1 affinity column-based IAC, PEGylated multi-walled carbon nanotubes, Fe_3O_4@COF(TAPT–DHTA) based MSPE

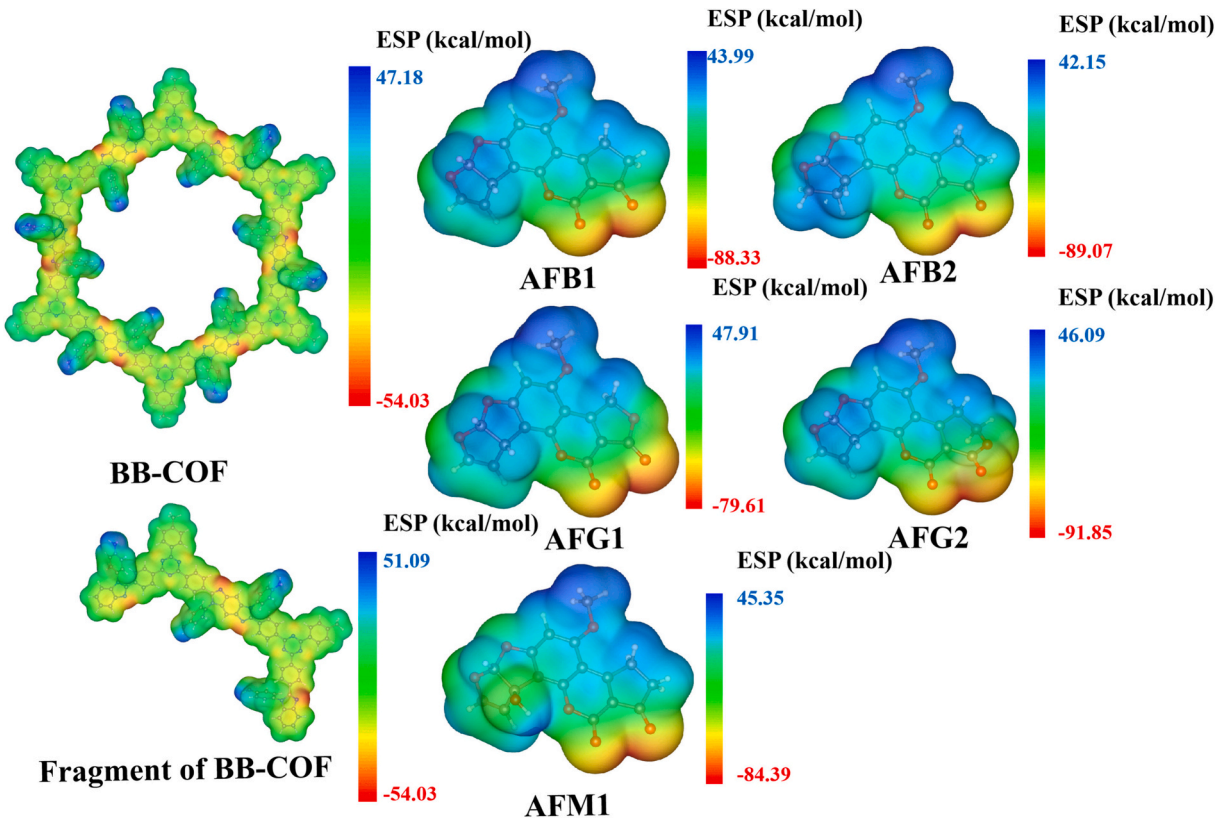

Fig. 6. The MESP of five AFs, BB-COF and fragment of BB-COF.

Table 1
Analytical performance of Fe_3O_4@BB-COF based MSPE-HPLC-MS/MS method for soybean, rice, corn, brown rice and buckwheat.

Sample	Analytes	Linear range (μg/kg)	R^2	LODs (μg/kg)	LOQs (μg/kg)	RSDs		ME
						Intraday (n = 5)	Interday (*n* = 5)	
Soybean	AFB1	0.20–20	0.9956	0.06	0.20	2.3	3.1	0.81
	AFB2	0.50–20	0.9970	0.15	0.50	3.1	5.2	0.91
	AFG1	0.30–20	0.9999	0.09	0.30	1.6	2.0	0.73
	AFG2	1.00–20	0.9955	0.29	1.00	1.9	7.1	1.01
	AFM1	0.80–20	0.9988	0.24	0.80	3.8	4.6	0.92
Rice	AFB1	0.90–20	0.9998	0.25	0.90	2.1	2.6	0.91
	AFB2	0.25–20	0.9990	0.07	0.25	1.7	3.1	0.90
	AFG1	0.50–20	0.9969	0.15	0.50	2.0	3.8	0.82
	AFG2	1.20–20	0.9985	0.36	1.20	1.9	5.7	0.65
	AFM1	1.00–20	0.9989	0.30	1.00	2.1	4.3	0.96
Corn	AFB1	0.45–20	0.9970	0.13	0.45	2.8	3.9	0.62
	AFB2	0.20–20	0.9980	0.06	0.20	1.9	4.0	0.68
	AFG1	1.00–20	0.9987	0.30	1.00	2.1	5.2	0.70
	AFG2	1.50–20	0.9969	0.45	1.50	2.5	5.1	0.79
	AFM1	0.50–20	0.9977	0.15	0.50	2.2	6.3	0.87
Brown rice	AFB1	0.10–20	0.9989	0.02	0.10	2.1	9.2	1.13
	AFB2	0.50–20	0.9990	0.13	0.50	3.2	10.2	1.09
	AFG1	0.05–20	0.9991	0.01	0.05	2.9	8.7	1.02
	AFG2	0.10–20	0.9982	0.02	0.10	6.1	7.5	0.83
	AFM1	0.05–20	0.9990	0.01	0.05	3.9	7.3	1.12
Buckwheat	AFB1	0.05–20	0.9976	0.01	0.05	5.3	8.1	0.92
	AFB2	0.50–20	0.9969	0.10	0.50	4.0	5.9	0.66
	AFG1	0.30–20	0.9991	0.08	0.30	2.5	5.1	0.80
	AFG2	0.80–20	0.9986	0.20	0.80	3.0	6.5	0.98
	AFM1	0.40–20	0.9995	0.12	0.40	3.1	8.2	0.99

Table 2
Recoveries of five AFs in soybean, rice, corn, brown rice and buckwheat samples.

Analyte	Added(μg/kg)	Soybean		Rice		Corn		Brown rice		Buckwheat	
		Recovery (%)	RSD (%)	Recovery (%)	RSD (%)	Recovery (%)	RSD (%)	Recovery (%)	RSD (%)	Recovery (%)	RSD (%)
AFB1	0	ND		ND		ND		ND		ND	
	2	85.2 ± 4.5	2.3	76.8 ± 2.6	3.0	90.1 ± 1.9	1.8	89.1 ± 3.6	5.6	80.3 ± 3.0	5.3
	5	90.1 ± 3.1	1.2	78.2 ± 3.4	2.1	86.3 ± 3.5	1.3	90.2 ± 2.5	4.2	79.8 ± 3.7	3.1
	20	91.3 ± 2.9	6.1	89.1 ± 2.5	1.1	88.0 ± 2.1	2.0	93.5 ± 2.8	3.0	90.0 ± 2.6	1.0
AFB2	0	ND		ND		ND		ND		ND	
	2	90.5 ± 1.1	2.6	79.2 ± 1.4	1.0	78.9 ± 1.6	1.6	80.2 ± 3.5	2.3	80.3 ± 3.0	3.3
	5	95.2 ± 1.9	2.9	81.9 ± 3.2	0.6	79.2 ± 1.6	2.4	90.2 ± 2.1	1.1	81.5 ± 2.3	2.0
	20	93.8 ± 4.1	1.7	92.8 ± 2.2	2.4	93.5 ± 0.7	1.7	95.1 ± 1.2	1.9	89.5 ± 1.9	2.1
AFG1	0	ND		ND		ND		ND		ND	
	2	91.6 ± 3.5	3.4	86.8 ± 0.9	1.4	97.1 ± 3.0	2.3	89.1 ± 4.0	5.6	92.8 ± 3.6	5.8
	5	92.5 ± 5.1	3.3	90.2 ± 3.1	1.0	89.0 ± 2.5	3.1	92.3 ± 2.1	6.1	89.6 ± 4.3	2.5
	20	92.5 ± 2.1	2.9	92.1 ± 2.8	2.5	88.0 ± 2.1	3.5	96.1 ± 0.6	2.0	93.1 ± 3.6	2.1
AFG2	0	ND		ND		ND		ND		ND	
	2	85.6 ± 0.6	2.1	92.4 ± 1.9	2.0	98.5 ± 1.5	1.1	89.9 ± 3.1	1.3	88.8 ± 4.1	4.0
	5	90.5 ± 2.1	1.8	95.1 ± 2.1	3.3	89.1 ± 1.3	2.2	88.7 ± 2.8	2.9	92.0 ± 2.2	3.2
	20	90.8 ± 3.1	3.1	93.0 ± 3.2	2.3	95.6 ± 2.0	1.7	94.1 ± 4.1	3.7	93.9 ± 1.8	2.5
AFM1	0	ND		ND		ND		ND		ND	
	2	83.1 ± 3.3	2.1	87.7 ± 3.1	1.7	85.3 ± 2.0	3.1	90.0 ± 4.0	5.0	86.5 ± 3.2	3.7
	5	86.9 ± 2.0	2.0	89.3 ± 4.2	2.1	78.1 ± 2.5	2.8	79.6 ± 3.8	2.2	88.9 ± 2.8	4.9
	20	93.1 ± 3.1	1.1	95.1 ± 2.7	0.9	91.7 ± 3.0	1.5	93.1 ± 2.9	1.2	92.7 ± 1.9	0.9

method, the LOQs achieved in this study was still lower than the maximum residue limits (2.0 μg/kg, and 4.0 μg/kg for AFB1 and total AFs) set by European Union for cereal samples. Overall, the aforementioned results indicate that the Fe_3O_4@BB-COF based MSPE-HPLC-MS/MS method exhibits simplicity, sensitivity, and reliability in the extraction and detection of AFs in soybean, rice, corn, brown rice, buckwheat samples, which could provide a valuable tool for ensuring food safety and quality control, particularly in the cereal industry.

4. Conclusion

The rich nitrogen-containing benzodiimidazole linkage magnetic COFs, (Fe_3O_4@BB-COF), with suitable polarity, were directly synthesized through a simple one-step cyclization and aromatization method. The Fe_3O_4@BB-COF exhibited excellent extraction performance for AFs due to synergistic interactions, involving pore-size matching effects, π-π interactions, hydrogen bonding interactions, polar interactions, electrostatic interactions and Lewis acid-base interactions. Utilizing Fe_3O_4@BB-COF as the magnetic adsorbent, a simple, efficient and reliable analytical method was developed for determination of five AFs in rice, wheat, corn, and soybean samples. This work has a promising application potential of Fe_3O_4@BB-COF in extraction of other polar food contaminants with some proper modifications. Nevertheless, strategies for the synergistic modification of multiple functional groups still require further exploration to improve the selectivity and applicability of the adsorbent for the sensitive reliable determination of AFs across a broader range of food matrices.

CRediT authorship contribution statement

Dan Wei: Writing – original draft, Validation, Funding acquisition, Formal analysis, Data curation, Conceptualization. **Jianliang Li:** Formal analysis, Project administration, Resources. **Shuangshuang Zheng:** Resources, Validation. **Ming Guo:** Formal analysis, Methodology, Resources, Validation. **Jingjing Xu:** Methodology, Resources, Validation. **Qiao Deng:** Conceptualization, Formal analysis, Funding acquisition, Methodology, Resources, Validation, Visualization. **Xu Wang:** Validation, Resources, Funding acquisition, Conceptualization.

Declaration of competing interest

The authors declare that they have no known competing financial interests or personal relationships that could have appeared to influence the work reported in this paper.

Data availability

Data will be made available on request.

Acknowledgments

This work was financially supported by the Natural Science Foundation of China (no. 32102077), the Natural Science Foundation of Hebei Province of China (no. B2021207002), the Zhejiang Provincial Natural Science Foundation of China (no. LTGY23B050004, LTGC23B050009), the Basic research project of Hangzhou Medical College (no. KYZD202101), the Key Laboratory of Biomarkers and In Vitro Diagnosis Translation of Zhejiang Province, the postdoctoral research project of Hebei Province (No. B2022005014) and the Key Discipline of Zhejiang Province in Public Health and Preventative Medicine (First Class, Category A), Hangzhou Medical College.

Appendix A. Supplementary data

Supplementary data to this article can be found online at https://doi.org/10.1016/j.fochx.2024.101797.

References

Annunziata, L., Stramenga, A., Visciano, P., Schirone, M., Colli, L. D., Colagrande, M. N., … Scortichini, G. (2017). Simultaneous determination of aflatoxins, T-2 and HT-2 toxins, and fumonisins in cereal-derived products by QuEChERS extraction coupled with LC-MS/MS. *Analytical and Bioanalytical Chemistry, 409*, 5143–5155. https://doi.org/10.1007/s00216-017-0462-z

Bagheri, A. R., Aramesh, N., Liu, Z., Chen, C., Shen, W., & Tang, S. (2022). Recent advances in the application of covalent organic frameworks in extraction: A review. *Critical Reviews in Analytical Chemitry*, 1–34. https://doi.org/10.1080/10408347.2022.2089838

Cheng, Y., Wang, B., Shen, J., Yan, P., Kang, J., Wang, W., Bi, L., Zhu, X., Li, Y., Wang, S., Shen, L., & Chen, Z. (2022). Preparation of novel N-doped biochar and its high adsorption capacity for atrazine based on π–π electron donor-acceptor interaction. *Journal of Hazardous Materials, 432*, Article 128757. https://doi.org/10.1016/j.jhazmat.2022.128757

Gomez, J. V., Tarazona, A., Mateo, F., Jimenez, M., & Mateo, E. M. (2019). Potential impact of engineered silver nanoparticles in the control of aflatoxins, ochratoxin a and the main aflatoxigenic and ochratoxigenic species affecting foods. *Food Control, 101*, 58–68. https://doi.org/10.1016/j.foodcont.2019.02.019

Hepsag, F., Golge, O., & Kabak, B. (2014). Quantitation of aflatoxins in pistachios and groundnuts using HPLC-FLD method. *Food Control, 38*, 75–81. https://doi.org/10.1016/j.foodcont.2013.10.005

Jia, M., Yu, L., Li, X., Li, Y., He, X., Chen, L., & Zhang, Y. (2023). An aptamerfunctionalized photonic crystal sensor for ultrasensitive and label-free detection of aflatoxin B1. *Talanta, 260*, Article 124638. https://doi.org/10.1016/j.talanta.2023.124638

Kuang, J., Ju, J., Lu, Y., Chen, Y., Liu, C., Kong, D., … Tang, S. (2023). Magnetic three-phase single-drop microextraction for highly sensitive detection of aflatoxin B1 in agricultural product samples based on peroxidase-like spatial network structure. *Food Chemistry, 416*, Article 135856. https://doi.org/10.1016/j.foodchem.2023.135856

Li, C. Y., Liu, J. M., Wang, Z. H., Lv, S. W., Zhao, N., & Wang, S. (2019). Integration of Fe_3O_4@UiO-66-NH_2@MON core-shell structured adsorbents for specific preconcentration and sensitive determination of aflatoxins against complex sample matrix. *Journal of Hazardous Materials, 384*, Article 121348. https://doi.org/10.1016/j.jhazmat.2019.121348

Li, J., Yang, Y., Zhou, Z., Li, S., Hao, L., Liu, W., Wang, Z., Wu, Q., & Wang, C. (2023). Fluorine-functionalized triazine-based porous organic polymers for the efficient adsorption of aflatoxins. *Journal of Agriculture and Food Chemiistry, 71*, 3068–3078. https://doi.org/10.1021/acs.jafc.2c08063

Li, S., Ma, J., Guan, J., Li, J., Wang, X., Sun, X., & Chen, L. (2023). Selective cationic covalent organic framework for high throughput rapid extraction of novel polyfluoroalkyl substances. *Journal of Hazardous Materials, 442*, Article 130125. https://doi.org/10.1016/j.jhazmat.2022.130125

Li, X. F., Jia, Z. M., Zhang, J., Zou, Y. D., Zhang, Y. D., Shu, K. W., … Ma, L. J. (2023). Regioselective one-step cyclization and aromatization towards directly amino-functionalized covalent organic framework with stable benzodiimidazole linkage. *Small, 19*, Article 2303775. https://doi.org/10.1002/smll.202303775

Liu, Y., Ling, Y., Zhang, Y., Feng, X., & Zhang, F. (2023). Synthesis of a magnetic covalent organic framework for extraction and separation of ultraviolet filters in beverage samples. *Food Chemistry, 410*, Article 135323. https://doi.org/10.1016/j.foodchem.2022.135323

Luan, T. X., Du, L., Wang, J. R., Li, K., Zhang, Q., Li, P. Z., & Zhao, Y. (2022). Highly effective generation of singlet oxygen by an imidazole-linked robust photosensitizing covalent organic framework. *ACS Nano, 16*, 21565. https://doi.org/10.1021/acsnano.2c10423

Ma, Y. F., Yao, Y. L., Qian, S. F., Deng, Z. K., Liu, Y., Ma, J. W., & Zhang, Z. L. (2024). Ball milling boosted hydrothermal N-doped sludge-derived biochar towards efficiently adsorptive removal of sulfamethoxazole from waters: Behavior, mechanism and DFT study. *Separation and Purification Technology, 338*, Article 126453. https://doi.org/10.1016/j.seppur.2024.126453

Maggira, M., Ioannidou, M., Sakaridis, I., & Samouris, G. (2021). Determination of afatoxin M1 in raw milk using an HPLC-FL method in comparison with commercial ELISA kits-application in raw milk samples from various regions of Greece. *Veterinary Science, 8*, 46. https://doi.org/10.3390/vetsci8030046

Martínez, J., Hernández-Rodríguez, M., Méndez-Albores, A., Téllez-Isaías, G., Jiménez, E. M., Nicolás-Vázquez, M., … Ruvalcaba, R. (2023). Computational studies of aflatoxin B1 (AFB1): A review. *Toxins, 15*(2), 135. https://doi.org/10.3390/toxins15020135

Nazhand, A., Durazzo, A., Lucarini, M., Souto, E. B., & Santini, A. (2020). Characteristics, occurrence, detection and detoxification of aflatoxins in foods and feeds. *Foods, 9*(5), 644. https://doi.org/10.3390/foods9050644

Nguyen, H. L., Gropp, C., Hanikel, N., Mockel, A., Lund, A., & Yaghi, O. M. (2022). Hydrazine-hydrazide-linked covalent organic frameworks for water harvesting. *ACS Central Science, 8*, 926. https://doi.org/10.1021/acscentsci.2c00398

Ni, B., Ye, J., Chen, J., Li, L., Liu, H., Wu, Y., & Wang, S. (2022). Surfactant-enhanced and automated pretreatment based on immunoaffinity magnetic beads coupled with ultra-performance liquid chromatography with fluorescence detection for the determination of aflatoxins in peanut oils. *Journal of Agriculture and Food Chemiistry, 70*, 10654–10661. https://doi.org/10.1021/acs.jafc.2c02529

Peng, Y., Zhang, S. W., Huang, J. H., Wu, C. L., Zhao, X. J., Feng, Y., & Gao, Y. H. (2024). Adaptive polarity of graphene oxide anchored silica doped with C18 for effective enrichment of aflatoxins from foodstuff. *Microchemical Journal, 197*, Article 109728. https://doi.org/10.1016/j.microc.2023.109728

Rezaeefar, A., Nemati, M., Farajzadeh, M. A., Afshar, M., Mogaddam, R., & Lotfipour, F. (2022). Development of N and S doped carbon sorbent-based dispersive micro solid phase extraction method combined with dispersive liquid-liquid microextraction for selected mycotoxins from soymilk samples. *Microchemical Journal, 173*, Article 107039. https://doi.org/10.1016/j.microc.2021.107039

Vijayalakshmi, S., Nadanasabhapathi, S., Kumar, R., & Kumar, S. S. (2018). Effect of pH and pulsed electric field process parameters on the aflatoxin reduction in model system using response surface methodology. *Journal of Food Science and Technology, 55*, 868–878. https://doi.org/10.1007/s13197-017-2939-3

Wang, B. X., Han, Y., Bai, Y. H., Lin, Z. G., Qiu, M. G., Nie, X. Y., … Wang, S. H. (2016). Effects of nitrogen metabolism on growth and aflatoxin biosynthesis in *aspergillus flavus*. *Journal of Hazardous Materials, 324*, 691. https://doi.org/10.1016/j.jhazmat.2016.11.043

Wang, C., Wang, Q. Q., Yu, J., Wang, X. M., Wang, L. J., Zhao, B., … Wu, Q. H. (2023). Converting waste expanded polystyrene into higher-value-added hyper-crosslinked porous polymer for rapid and high-efficient adsorption of aflatoxins. *Journal of Cleaner Production, 408*, Article 137102. https://doi.org/10.1016/j.jclepro.2023.137102

Wang, C. H., Li, J., Wang, Q. Q., Wu, Q. H., & Shi, X. D. (2023). Fluorine-functionalized covalent organic framework as efficient solid phase extraction sorbent for adsorption of aflatoxins in nuts. *Journal of Hazardous Materials, 464*, Article 133017. https://doi.org/10.1016/j.jhazmat.2023.133017

Wang, J., Huang, Q. W., Guo, W. B., Guo, D. K., Han, Z., & Nie, D. X. (2023). Fe_3O_4@COF (TAPT-DHTA) nanocomposites as magnetic solid-phase extraction adsorbents for simultaneous determination of 9 mycotoxins in fruits by UHPLC-MS/MS. *Toxins, 15*, 117. https://doi.org/10.3390/toxins15020117

Wang, N., Li, W. H., Cheng, W. Q., Wang, Y., Zheng, Z., Hu, X. Y., … Zheng, Z. (2023). Guest adaptative supramolecular sensing strategy for warning the risky aflatoxins in contaminated cereals. *Journal of Hazardous Materials, 464*, Article 133015. https://doi.org/10.1016/j.jhazmat.2023.133015

Wang, Q. Q., Zhang, S. H., Lia, Z., Wang, Z., Wang, C., Alshehric, S., … Wu, Q. H. (2022). Design of hyper-cross-linked polymers with tunable polarity for effective preconcentration of aflatoxins in grain. *Chemical Engineering Journal, 453*, Article 139544. https://doi.org/10.1016/j.cej.2022.139544

Xu, H., Sun, J., Wang, H., Zhang, Y., & Sun, X. (2021). Adsorption of aflatoxins and ochratoxins in edible vegetable oils with dopamine-coated magnetic multi-walled carbon nanotubes. *Food Chemistry, 365*, Article 130409. https://doi.org/10.1016/j.foodchem.2021.130409

Yang, J., Huang, L. J., You, J. M., & Yamauchi, Y. (2023). Magnetic covalent organic framework composites for wastewater remediation. *Small, 19*, Article 2301044. https://doi.org/10.1002/smll.202301044

Yang, Y., Guo, Y., Jia, X., Zhang, Q., Mao, J., Feng, Y., Yin, D., Zhao, W., Zhang, Y., Ouyang, G., & Zhang, W. (2023). An ultrastable 2D covalent organic framework coating for headspace solid-phase microextraction of organochlorine pesticides in environmental water. *Journal of Hazardous Materials, 452*, Article 131228. https://doi.org/10.1016/j. jhazmat.2023.131228

Yang, Y., Ma, X., Li, Z., Wang, Y., Ju, C., Cao, L., Zheng, Y., & Zhang, Q. (2023). ZIF-8 and humic acid modified magnetic corn stalk biochar: An efficient, magnetically stable, and eco-friendly adsorbent for imidacloprid and thiamethoxam removal. *Chemical Engineering Journal, 465*, Article 142788. https://doi.org/10.1016/j.cej.2023.142788

Yu, L., Li, P., Zhang, Q., Zhang, W., Ding, X., & Wang, X. (2013). Graphene oxide: An adsorbent for the extraction and quantification of aflatoxins in peanuts by high-performance liquid chromatography. *Journal of Chromatography A, 1318*, 27–34. https://doi.org/10.1016/j.chroma.2013.10.006

Zhao, Y., Chen, D., Duan, H. Y., Li, P. W., Wu, W. Q., Wang, X. P., … Zhang, Z. W. (2023). Sample preparation and mass spectrometry for determining mycotoxins, hazardous fungi, and their metabolites in the environment food, and healthcare. *Trac-Trends in Analytical Chemistry, 160*, Article 116962. https://doi.org/10.1016/j.trac.2023.116962

Zhao, Y., Yuan, Y. C., Bai, X. L., Liu, Y. M., Wu, G. F., Yang, F. S., & Liao, X. (2020). Multi-mycotoxins analysis in liquid milk by UHPLC-Q exactive HRMS after magnetic solid-phase extraction based on PEGylated multi-walled carbon nanotubes. *Food Chemistry, 305*, Article 125429. https://doi.org/10.1016/j.foodchem.2019.125429

Zhou, F. L., Deng, H. L., Agarry, I. E., Hu, J., Xu, D. H., Feng, H., … Chen, K. W. (2023). Determination of multiple mycotoxins in chili powder using cold-induced liquid–liquid extraction and Fe_3O_4@MWCNTs-NH_2 coupled with UPLC-Q-TOF/MS. *Food Chemistry, 423*, Article 136291. https://doi.org/10.1016/j.foodchem.2023.136291